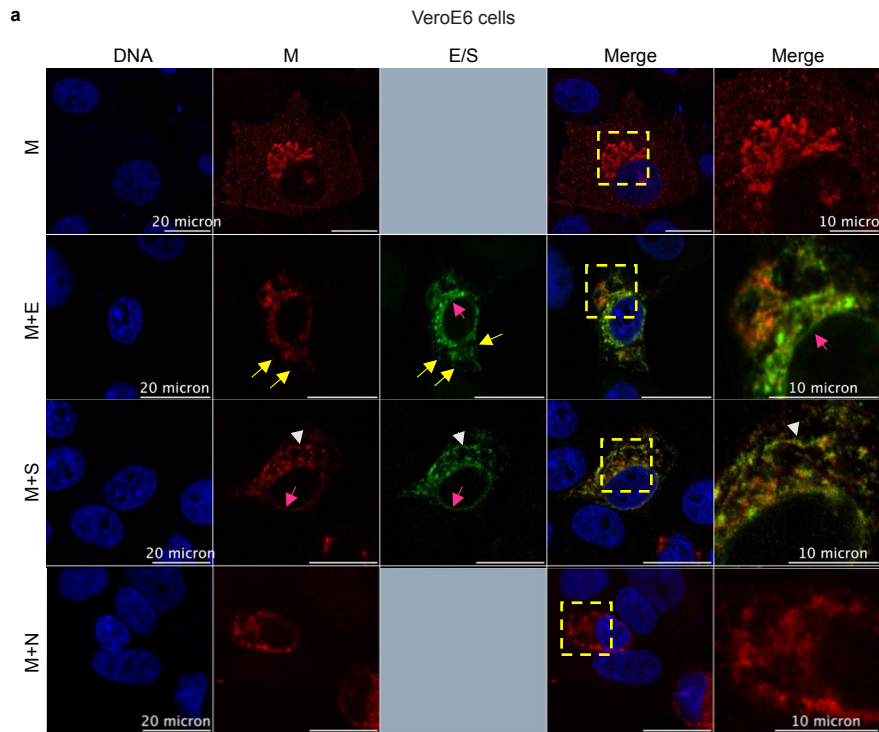


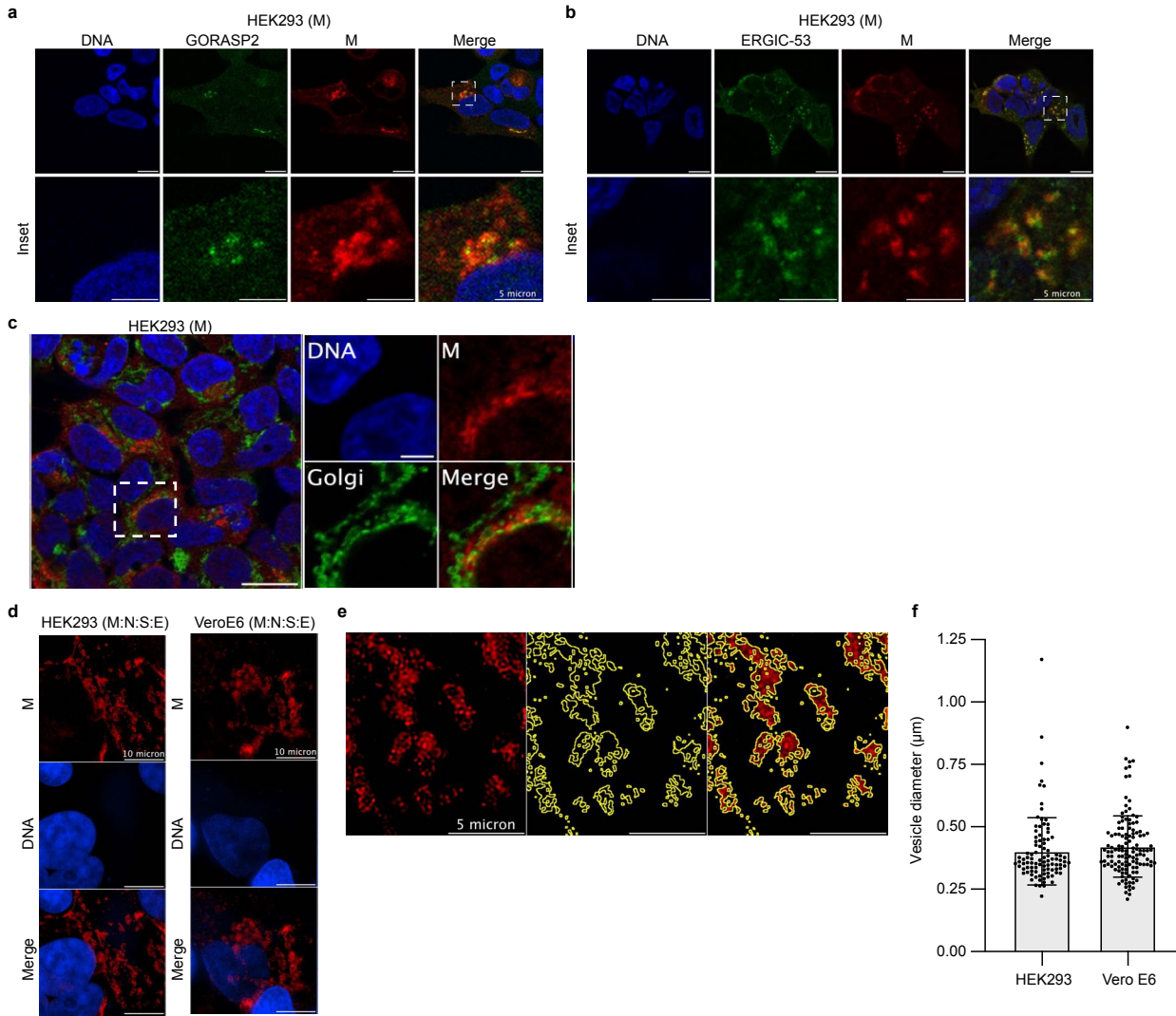
**Supplementary Figure 1. M protein-lipid interactions.**

(a) Sphingolipid, (b) lipid, and (c) phosphatidylinositol snooper assays for M-lipid interactions. (a) Western blots of immobilized lipids probed with HA-tagged M, a 50:50 mixture of EGFP-tagged:untagged M, His- and Sumo-tagged M, or a control without M protein. All M constructs tested displayed strong binding to C1P and dihydroC1P as well as appreciable binding to anionic So1P and Sa1P. Lipid and (b,c) Western blots of immobilized lipids probed with His- and Sumo-tagged M. No appreciable binding is observed. All westerns were performed with anti-M antibody and secondary conjugated to HRP. Portions of (a) are reproduced from Fig. 1a.



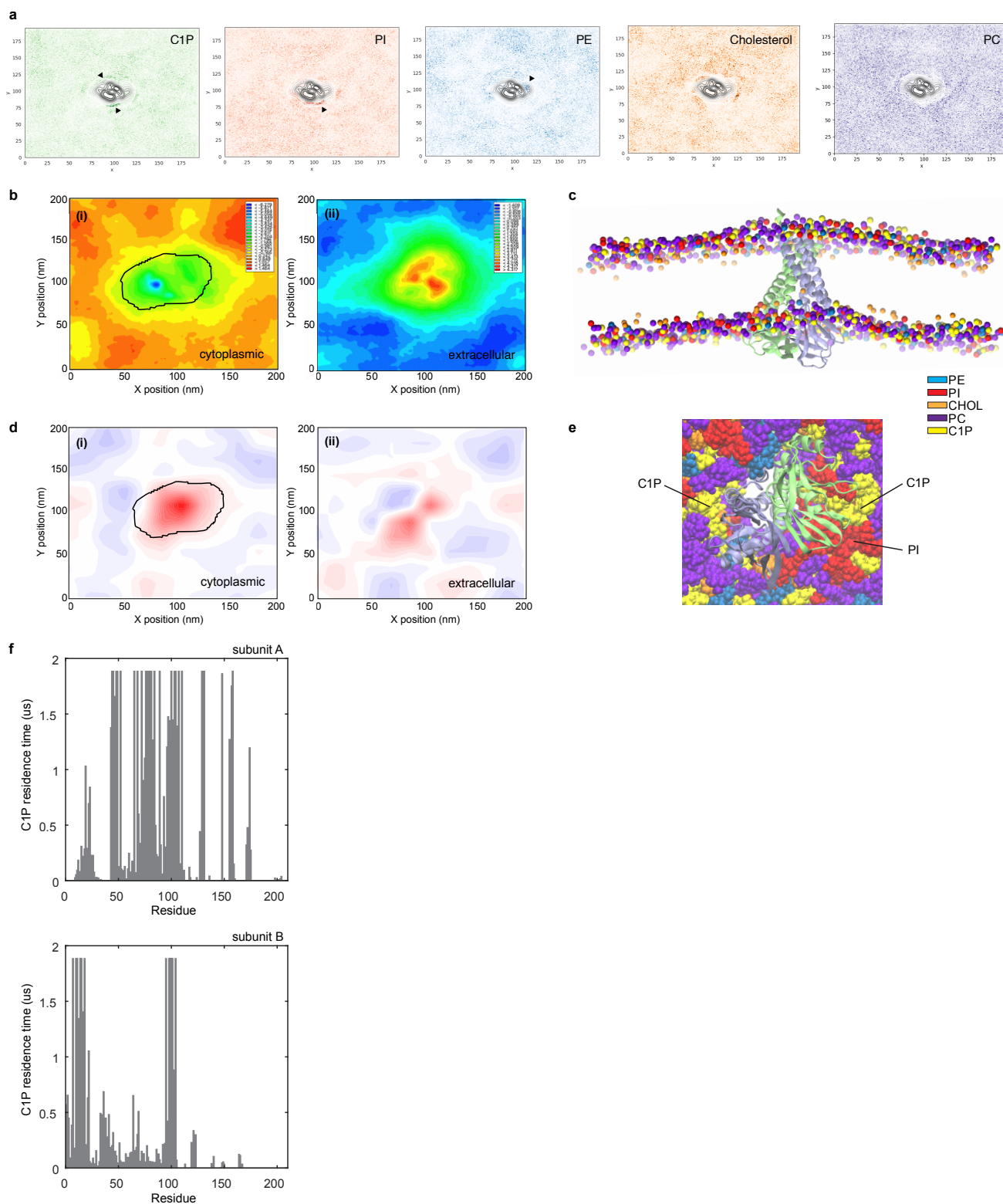
**Supplementary Figure 2. SARS-CoV-2 M colocalizes with S and E proteins.**

Vero E6 cells were used to assess M protein localization when co-expressed with E, S, or N. The insets and arrows show regions of colocalization.



**Supplementary Figure 3. SARS-CoV-2 M colocalizes with Golgi and ERGIC markers and SARS-CoV-2 structural proteins co-expressed in mammalian cells exhibit similar vesicle morphology to SARS-CoV-2 infected cells.**

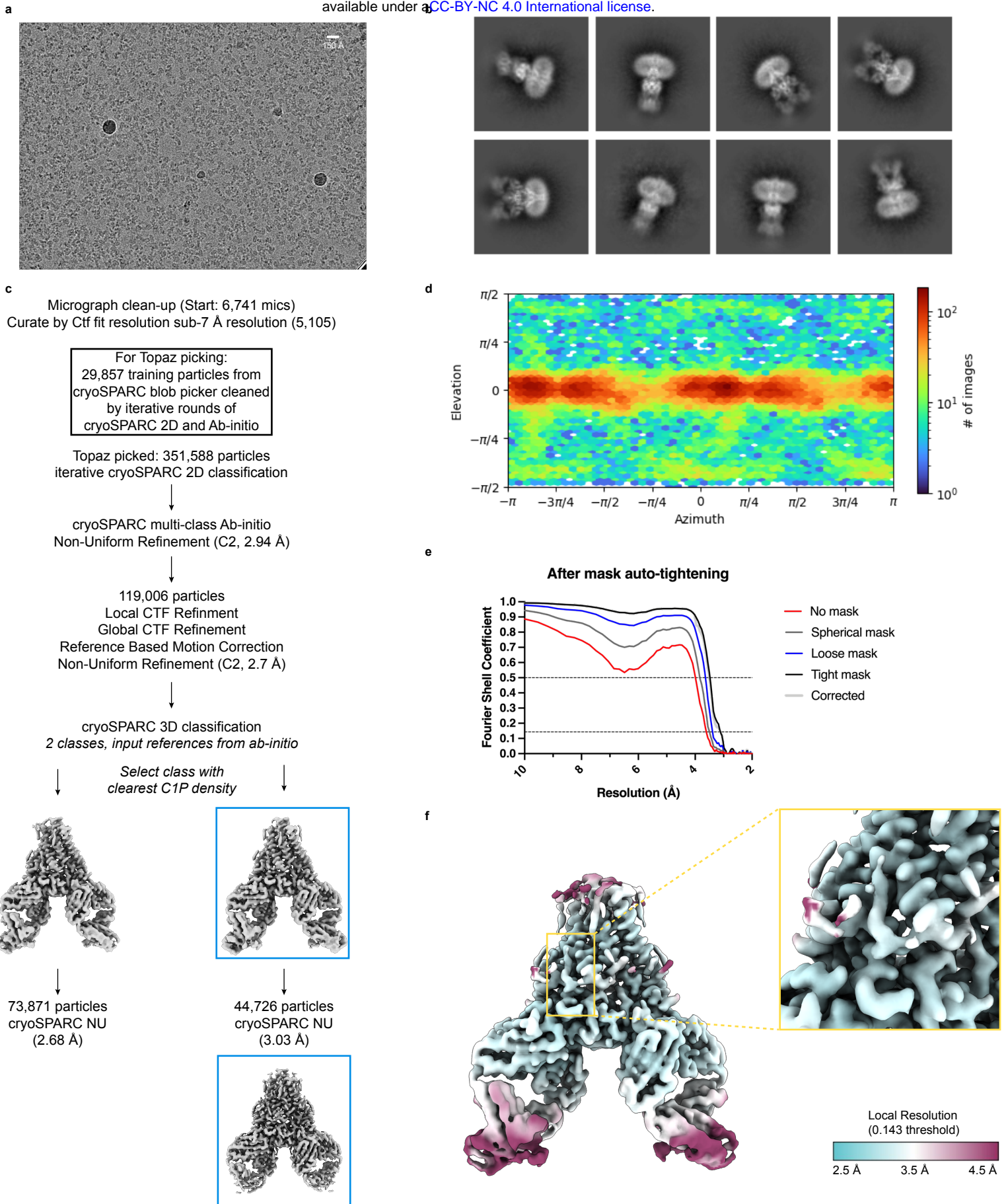
(a) WT M protein (red) expressed in HEK293 cells colocalized with the Golgi GORASP2 marker (green). (b) WT M protein (red) expressed in HEK293 cells colocalized with the ERGIC-53 marker (green). (c) WT M protein (red) expressed in HEK293 cells did not appreciably colocalize a ER marker (green) (c) SARS-CoV-2 structural proteins (S, M, Flag-E, and N) were co-expressed in HEK293 or Vero E6 cells and imaged with structure illuminated microscopy using a Nikon N-STORM/N-SIM/TIRF imaging system. Immunofluorescence with labelled anti-Flag antibody for detection of the Flag-E protein (red). (e) A zoomed in portion of (d) is shown to demonstrate how vesicle diameter was quantified. (f) Quantification of vesicle size was performed using ImageJ. Similar average vesicle diameters illuminated with E-Flag antibody were found in HEK293 and Vero E6 cells.



**Supplementary Figure 4. Lipid density maps, membrane response, and M-C1P residence time from molecular dynamics simulations.**

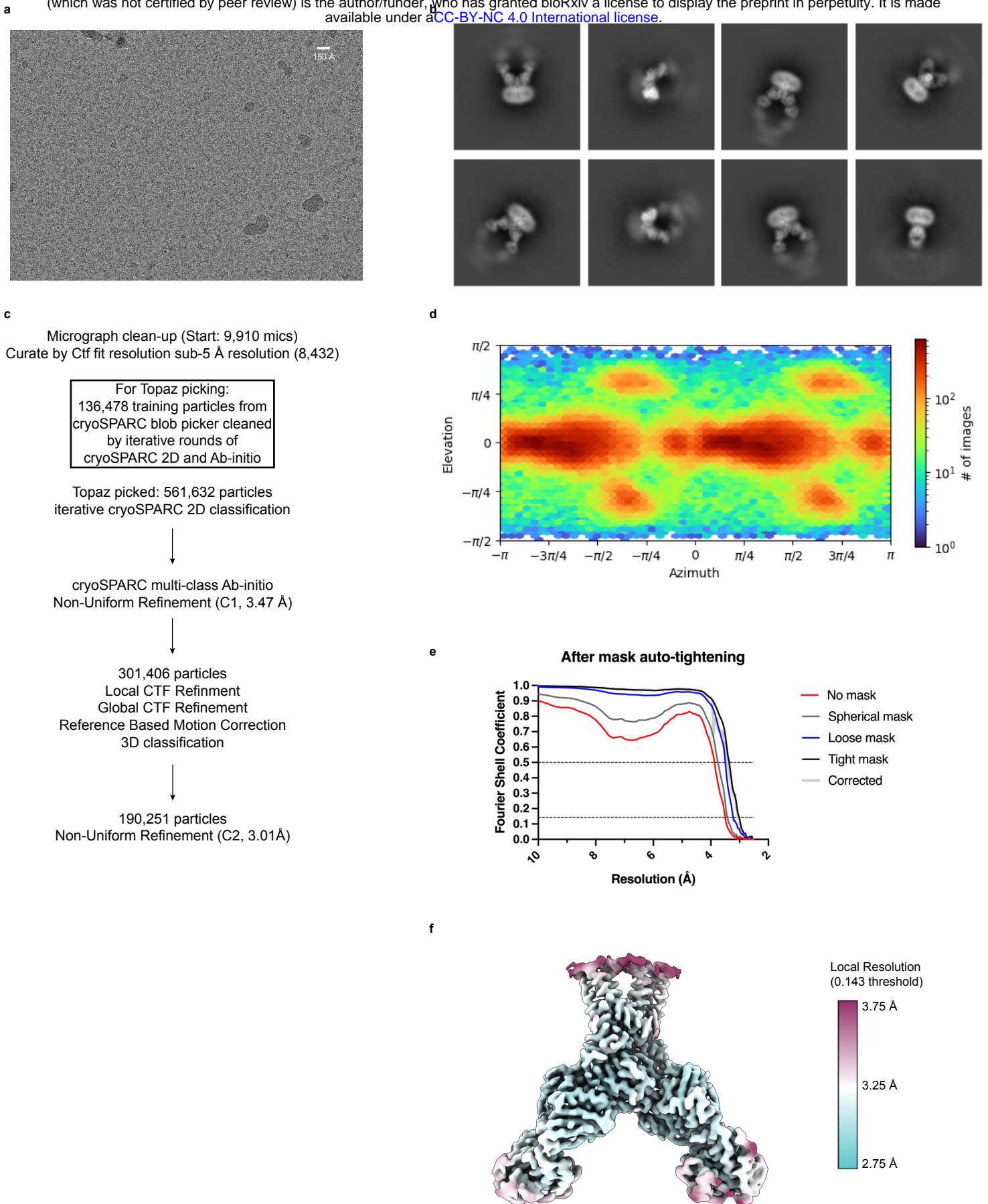
(a) Density for C1P, POPI, DYPE, cholesterol, and PC in the simulation box is illustrated with darker color indicating higher density. Arrowheads indicate higher lipid accumulation. The central region corresponds to M protein. (b) Z-coordinates of lipid head groups averaged over the last 2  $\mu$ s of trajectories and mapped into the XY plane for outer (i) and inner (ii) leaflets. The black circle in the top leaflet highlights the region of membrane thinning. (c) Side view of the simulated  $M_{short}$  box. Membrane thinning is apparent around M protein. (d) Mean curvature of the membrane mapped onto the XY plane for outer (i) and inner (ii) leaflets showing small deformations around M from a nearly flat surface. (e) Accumulation of C1P and PI lipids in proximity to  $M_{short}$ . (f) Residence time of C1P by residue in subunit A (above) and subunit B (below).





**Supplementary Figure 5. Cryo-EM data, processing pipeline, and validation for  $M_{short}$ -C1P.**

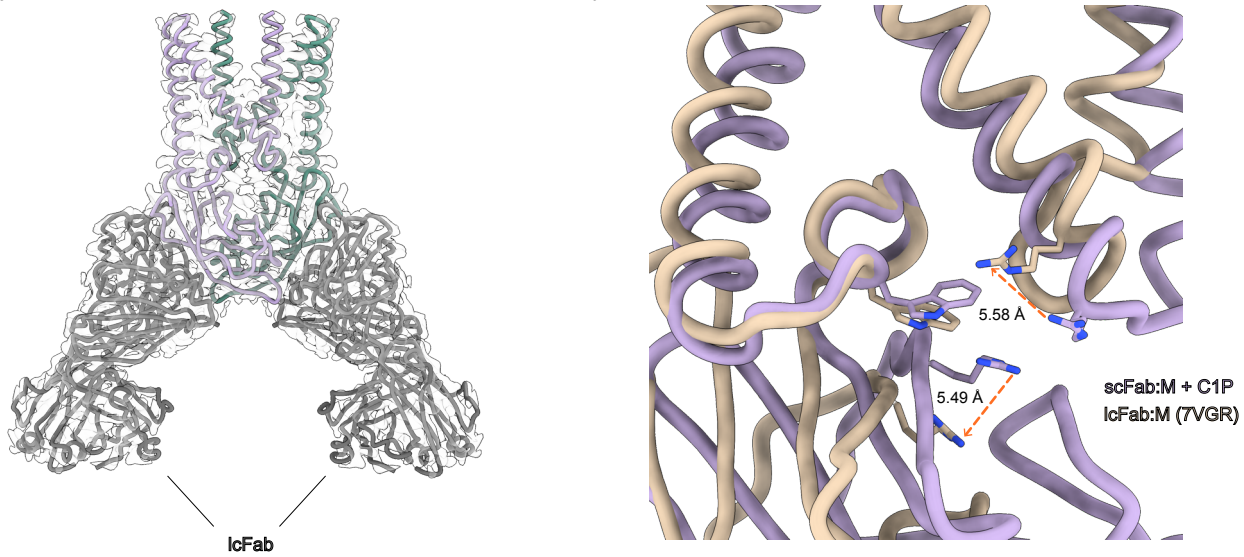
(a) Representative micrograph, (b) selected 2D class averages, (c) cryo-EM data processing pipeline, (d) view angle distribution, (e) Fourier shell correlation (FSC) versus resolution between half maps from final non-uniform refinement, and (f) local resolution drawn on final sharpened map with inset zoomed in on C1P binding site.



**Supplementary Figure 6. Cryo-EM data, processing pipeline, and validation for  $M_{long}$  in the presence of C1P.**

(a) Representative micrograph, (b) selected 2D class averages, (c) cryo-EM data processing pipeline, (d) view angle distribution, (e) Fourier shell correlation (FSC) versus resolution between half maps from final non-uniform refinement, and (f) local resolution drawn on final sharpened map.

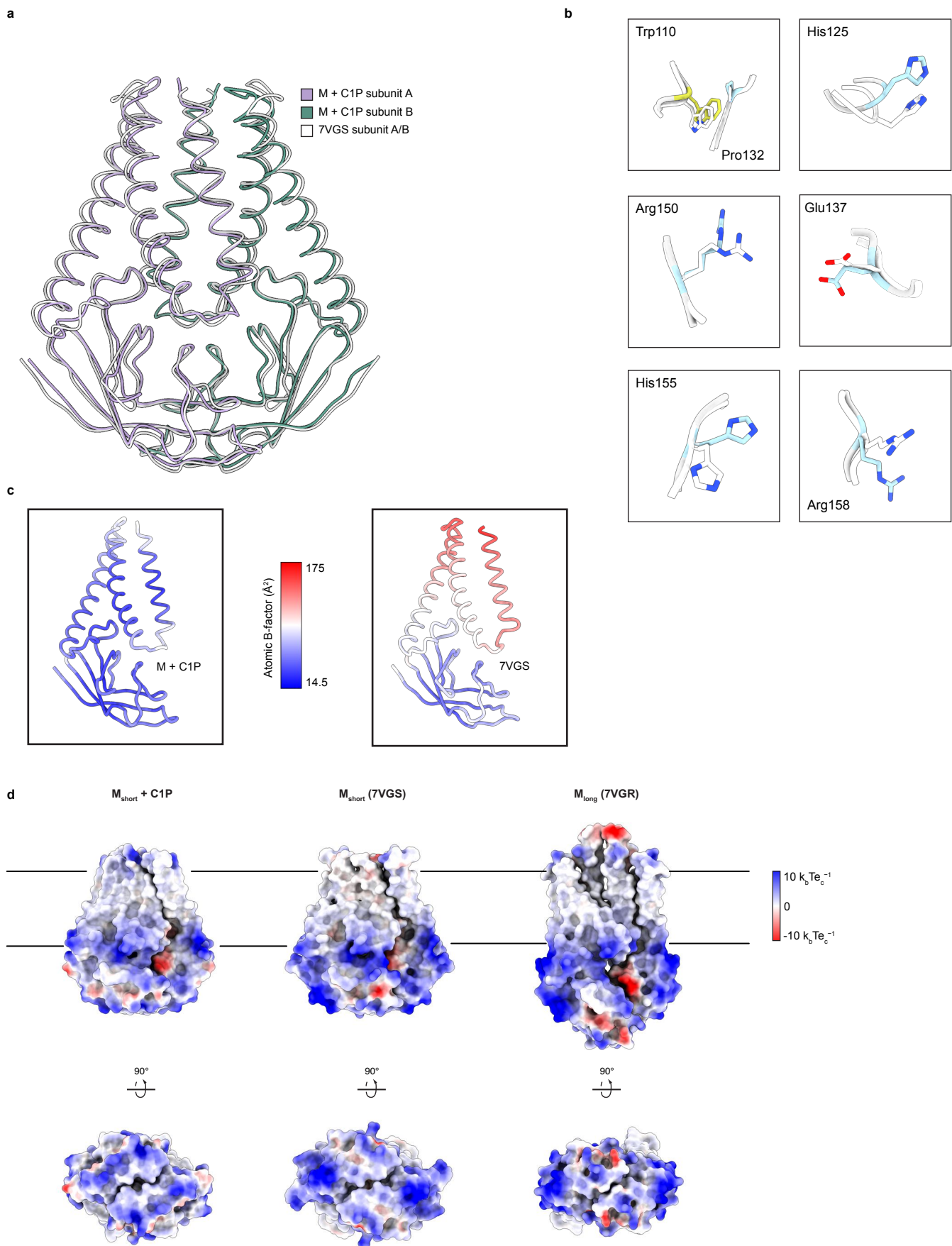
a



**Supplementary Figure 7. Structure of M<sub>long</sub> in the presence of C1P.**

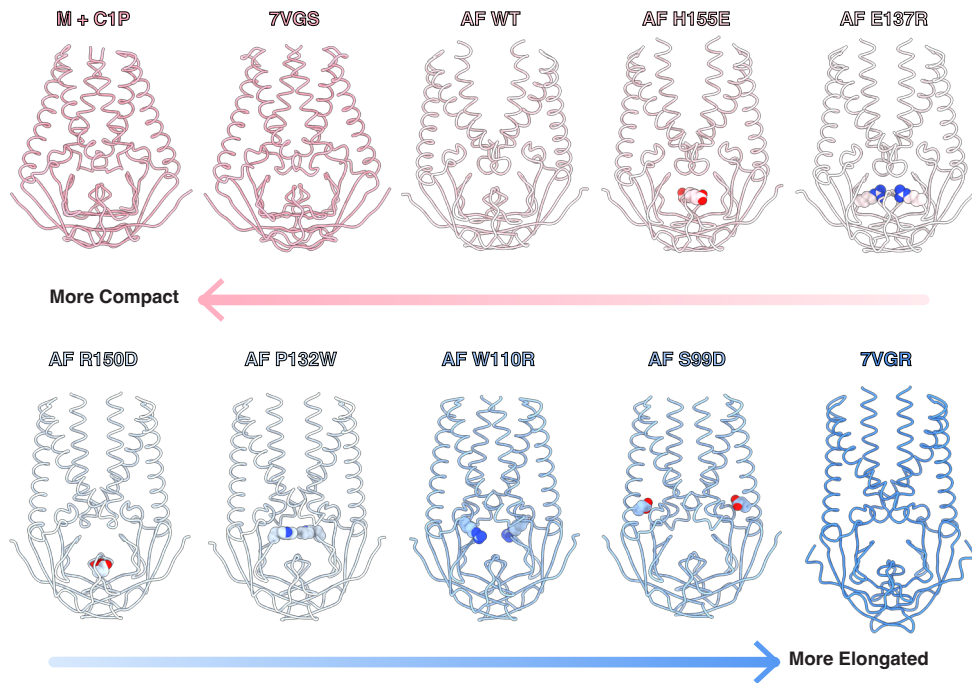
(a) Final model M<sub>long</sub> conformation viewed from the membrane. M subunits are purple and green and long conformation-selective Fabs are gray. 3.0 Å resolution sharpened map is shown as a transparent surface. (b) Overlay of M<sub>long</sub> + C1P and M<sub>short</sub>-C1P structures highlighting rearrangement of the C1P binding site observed in M<sub>short</sub> including relative displacement of key C1P-interacting residues.





**Supplementary Figure 8. C1P binding compacts and stabilizes  $M_{\text{short}}$**

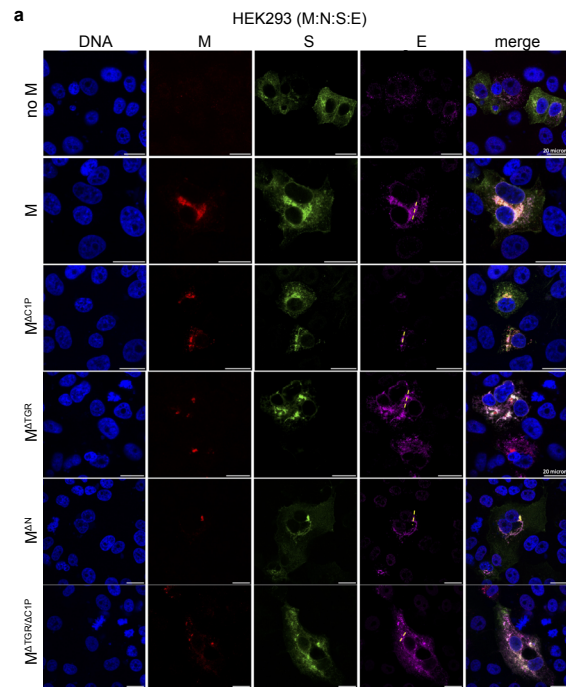
(a) Overlay of  $M_{\text{short}} + \text{C1P}$  (colored purple and green) and apo  $M_{\text{short}}$  illustrating compaction of transmembrane region. (b) Overlay of selected hinge and CTD residues from  $M_{\text{short}} + \text{C1P}$  (blue) and apo  $M_{\text{short}}$  structures. (c) Single subunit from  $M_{\text{short}} + \text{C1P}$  (left) and apo  $M_{\text{short}}$  (right) structures colored by refined B-factor. (d)  $M_{\text{short}} + \text{C1P}$  (left), apo  $M_{\text{short}}$  and  $M_{\text{long}}$  electrostatic surface potential.



**Supplementary Figure 9. Mutations are predicted to shift M protein conformational landscape.**

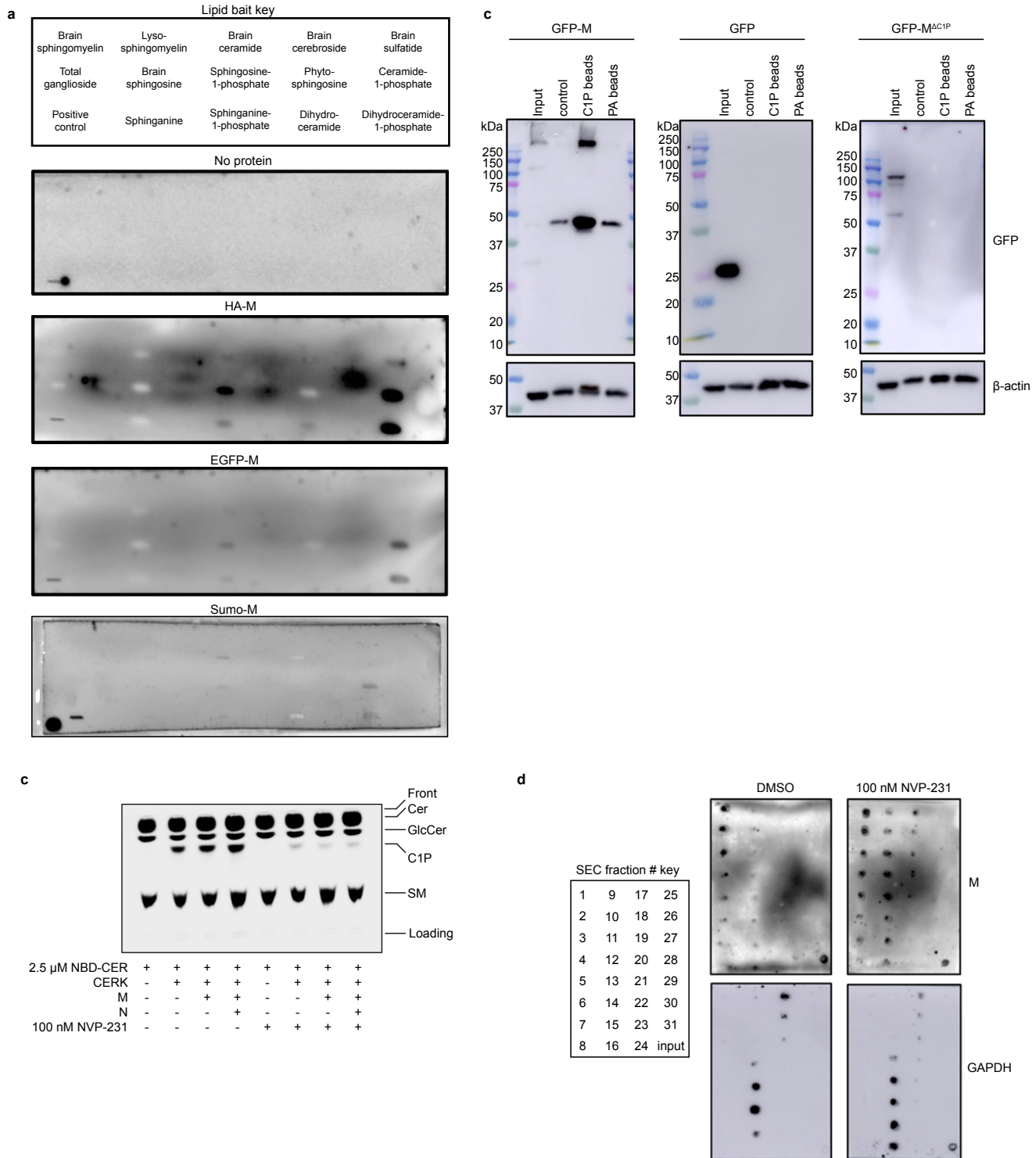
Comparison of experimentally determined ( $M_{short}$ -C1P, apo  $M_{short}$  and  $M_{long}$ ) and AlphaFold3-predicted (AF wild-type M, H155E, E137R, R150D, P132W, W110R, and S99D) structures. Mutated sites are drawn as spheres. Mutations were hypothesized to destabilize  $M_{short}$  based on  $M_{short}$ -C1P and  $M_{short}$ -JNJ-9676 structures. Models are arranged and colored from pink (most compact) to white (intermediate between short and long conformations) to blue (most elongated).





**Supplementary Figure 10. Colocalization of SARS-CoV-2 structural proteins in cells.**

HEK293 cells transfected with S,E,N, and M constructs used in this study and immunostained for M, S, and E



**Supplementary Figure 11. Uncropped blot and thin-layer chromatography images.**

(a) Sphingolipid snoper blot (Fig. 1A), (b) lipid-coated bead pull down blots (Figs. 1b, 4c), (c) CERK inhibition by NVP-231 assessed by TLC (Fig. 1e), and (d) blot of size chromatography fractionated lysates from DMSO- or NVP-231- treated cells expressing M, N, E, and S (Fig. 1e).